

Geophysical Research Letters[®]

RESEARCH LETTER

10.1029/2025GL117802

Seismogenic Thickening in the Pamir Plateau From Craton Underthrusting Revealed by the 2023 Mw 6.9 Earthquake

Qingyi Liu^{1,2}, Yingfeng Zhang¹, Zhangfeng Ma³, Luca Dal Zilio^{3,4}, Guohong Zhang⁵, Hongyi Li², and Xinjian Shan⁵

¹Xinjiang Pamir Intracontinental Subduction National Observation and Research Station, Institute of Geology, China Earthquake Administration, Beijing, China, ²Key Laboratory of Intraplate Volcanoes and Earthquakes, China University of Geosciences (Beijing), Ministry of Education, Beijing, China, ³Earth Observatory of Singapore, Nanyang Technological University, Singapore, Singapore, ⁴Asian School of the Environment, Nanyang Technological University, Singapore, Singapore, ⁵State Key Laboratory of Earthquake Dynamics, Institute of Geology, China Earthquake Administration, Beijing, China

Key Points:

- The 2023 Mw6.9 Pamir earthquake exhibits mainly left-lateral strike-slip motion, consistent with past large High Pamir Plateau earthquakes
- The cold, rigid cratonic lithosphere likely causes deeper coseismic rupture beneath the High Pamir than in the Tibetan Plateau
- Earthquake and geodetic data reveal a broadly distributed shear zone above the leading edge of the underthrusting Indian plate

Supporting Information:

Supporting Information may be found in the online version of this article.

Correspondence to:

Y. Zhang,
jingqing129@ies.ac.cn

Citation:

Liu, Q., Zhang, Y., Ma, Z., Zilio, L. D., Zhang, G., Li, H., & Shan, X. (2025). Seismogenic thickening in the Pamir Plateau from craton underthrusting revealed by the 2023 Mw 6.9 earthquake. *Geophysical Research Letters*, 52, e2025GL117802. <https://doi.org/10.1029/2025GL117802>

Received 1 JUL 2025
Accepted 23 NOV 2025

Author Contributions:

Conceptualization: Qingyi Liu, Yingfeng Zhang, Luca Dal Zilio, Guohong Zhang

Data curation: Zhangfeng Ma

Formal analysis: Guohong Zhang, Hongyi Li, Xinjian Shan

Investigation: Zhangfeng Ma, Luca Dal Zilio, Guohong Zhang, Hongyi Li, Xinjian Shan

Methodology: Zhangfeng Ma, Luca Dal Zilio, Guohong Zhang, Hongyi Li, Xinjian Shan

Project administration: Yingfeng Zhang

Software: Qingyi Liu, Zhangfeng Ma

Abstract The convergence of the Indian and Eurasian plates beneath the Pamir Plateau has produced complex continental subduction, significantly influencing upper crustal faulting and seismicity. To investigate the kinematic behavior of the High Pamir Plateau, we derive a geodetic slip model for the 2023 Mw 6.9 Pamir earthquake by using Sentinel-1A and ALOS-2 InSAR data. Our geodetic inversion reveals rupture along two distinct faults: a dominant left-lateral strike-slip fault and a secondary normal fault, consistent with the mechanisms of the 1911 Mw 7.3 and 2015 Mw 7.2 earthquakes in the region. Notably, the 2015 and 2023 ruptures extend to ~20 km depth—deeper than typical Tibetan Plateau earthquakes—likely due to the thermal influence of the underlying cratonic lithosphere. Our results also indicate a broad shear zone above the underthrusting Indian plate, underscoring the role of lithospheric-scale dynamics in shaping crustal fault behavior in the Pamir region.

Plain Language Summary We used comprehensive satellite radar data sets to analyze the 2023 Mw 6.9 earthquake in the Pamir Plateau. The results show that the earthquake ruptured two faults—a main left-lateral strike-slip fault and a secondary normal fault—consistent with previous large earthquakes in the region. Unlike typical shallow earthquakes on the Tibetan Plateau, this event extended to depths of about 20 km. This deeper rupture likely reflects the influence of the cold, strong lithosphere beneath the Pamir, part of the underthrusting Asian craton. Our findings highlight how deep tectonic processes can control the location and nature of earthquakes near the surface.

1. Introduction

The complex geodynamic and tectonic evolution of a region is a key factor shaping its slip partitioning and seismic activity (Rutte et al., 2017; Schurr et al., 2014). Recent multi-scale models have bridged long-term tectonic and geodynamic processes with the shorter-term evolution of stress and slip across multiple earthquake cycles (Dal Zilio et al., 2019; Lavier et al., 2021). However, it remains challenging to understand how lithosphere-to-mantle-scale processes influence fault dynamics over seismic-cycle timescales.

The Pamir Plateau, located in the northwest of the India-Eurasia collision system, offers a compelling region for studying mountain-building processes and associated earthquake behaviors, owing to its complex three-dimensional continental subductions (Bloch et al., 2021; Burtman & Molnar, 1993; Fan et al., 1994). Focal mechanisms delineate an arc-shaped convergent belt, similar to those seen in the Himalayas (Sippl, Schurr, Yuan, et al., 2013). The interior of the plateau exhibits a heterogeneous stress regime, characterized by the interplay of shear and extensional forces (Bloch et al., 2023; Burtman & Molnar, 1993; Cowgill, 2010; Fan et al., 1994; Kufner et al., 2016; Murphy et al., 2000; Schurr et al., 2014; Schwab et al., 2004), which are associated to gravitational potential, horizontal compression, and deep subduction processes (Schurr et al., 2014).

Recently, a moment magnitude (Mw) 6.9 earthquake, hereafter referred to as the “2023 Pamir earthquake,” ruptured the largest strike-slip fault system in the interior of the Pamir Plateau, the Sarez-Karakul Fault System (SKF). Following the 2015 Mw 7.2 Sarez earthquake, which was recorded by modern observations, including seismometers (Bloch et al., 2023) and remote sensing imagery (Jin et al., 2022), the 2023 Mw 6.9 Pamir

© 2025. The Author(s).

This is an open access article under the terms of the [Creative Commons Attribution-NonCommercial-NoDerivs License](#), which permits use and distribution in any medium, provided the original work is properly cited, the use is non-commercial and no modifications or adaptations are made.

Supervision: Guohong Zhang, Hongyi Li
Validation: Yingfeng Zhang,
 Zhangfeng Ma, Luca Dal Zilio, Hongyi Li
Visualization: Qingyi Liu
Writing – original draft: Qingyi Liu
Writing – review & editing: Qingyi Liu,
 Yingfeng Zhang, Zhangfeng Ma, Luca
 Dal Zilio, Hongyi Li

earthquake represents the largest and most destructive event to have occurred in the region. Together, the 2015 and 2023 earthquakes provide new insights into the kinematic and dynamic connections between the continental subduction processes beneath the Pamir and the above crustal earthquake behaviors.

In this study, we aim to investigate the kinematic behavior of the High Pamir Plateau by first developing detailed kinematic models for both the 2015 Sarez and 2023 Pamir earthquakes, based on geodetic data. We further compile available interseismic InSAR and GNSS velocity measurements to assess long-term deformation patterns across the region. Finally, we analyze the underlying mechanisms driving the current tectonic movements of the plateau, linking them to deep-seated subduction processes beneath the crust. Our results highlight significant thickening of the seismogenic zone, likely driven by the underthrusting of the Indian craton.

2. Tectonic Settings

The low Pamir Plateau is dominated by thrust earthquakes, whereas the high Pamir Plateau frequently experiences both strike-slip and normal faulting earthquakes (Figure 1a, Murphy et al., 2000; Strecker et al., 1995; Yin et al., 2001). In this study, we focus exclusively on earthquakes with hypocenters shallower than 30 km to minimize the influence of deep continental subduction. Prominent earthquakes in the high Pamir Plateau, such as the 1911 M 7.2, 2015 Mw 7.2, and 2023 Mw 6.9 events (Figure 1), exhibited significant strike-slip motion along the SKF and near the Sarez-Murghab Thrust Fault System (SMTF, Elliott et al., 2020; Jin et al., 2022; Sangha et al., 2017).

The SKF is the main strike-slip fault in the high Pamir Plateau (Figure 1a), extending from Sarez Lake in the south to the Main Pamir Thrust Fault Belt in the north. The SKF fault system marks a boundary with contrasting topographic and seismic features: the eastern side has relatively flat terrain and infrequent destructive earthquakes, whereas the western side exhibits higher topographic relief and elevated seismicity (Schurr et al., 2014). Both the 2015 and 2023 earthquakes ruptured segments of the SKF located south of the SMTF. In this region, the SKF features several branches, reflecting significant distributed shear strain (Sippl, Schurr, Yuan, et al., 2013).

The SMTF is a major active fault system within the Pamir Plateau (Figure 1b), marking its central and southern regions and reactivating the Russhan-Pshart Suture zone (Schurr et al., 2014), which is a remnant of a closed and vanished ancient ocean along the southern margin of the Central Pamir block (S. Wang et al., 2020). This system intersects with the dextral strike-slip SKF. The eastern segment of SMTF, located in the high-seismicity zone east of Lake Sarez, contains multiple active fault bands and deep seismic zone, which likely indicate the intrusion of the Indian craton boundary (Kufner et al., 2016, 2018; Schurr et al., 2014). The 2015 and 2023 earthquakes occurred along this boundary.

Intermediate-depth seismicity within the Pamir Plateau is concentrated in a curved area extending southwest along the SKF fault system, with intense activity in the deepest part of the Hindu Kush range (Figure 1a, Bai & Zhang, 2015; Kufner et al., 2016; Pegler & Das, 1998; Zhan & Kanamori, 2016; Zhang et al., 2011). This region may mark the convergence zone between the Eurasian and Indian Plates, though the precise dynamics of their collision remain debated. The eastern Pamir region is influenced by the northward advance of the Indian lithosphere, while the western side is shaped by the collision between the northern Eurasian Plate and the southern Indian Plate at the Hindu Kush (Figure 1c, Bloch et al., 2021; Kufner et al., 2018; Perry et al., 2019; J. Zhao et al., 2021). Intermediate-depth seismicity highlights a complex convergence pattern between these cratons, though the specifics of their interaction remain a subject of ongoing debate.

3. Method

3.1. InSAR Data Process

We mapped the coseismic deformation of the 2023 Pamir earthquake using both ascending and descending Sentinel-1A SAR data. The data set includes all Single Look Complex scenes acquired within 1 year before and after the event. Interferometric processing was performed using the CtSent toolbox (Ma et al., 2019, 2020, 2021, 2022) for TOPS-mode Sentinel-1A data (Text S1 in Supporting Information S1).

Multilooking was applied with factors of 10 (azimuth) \times 40 (range), and the topographic phase was removed using the 90 m SRTM DEM. We employed the InSAR Stacking technique to generate the coseismic deformation field (See Text S2 in Supporting Information S1 for details). This process involved selecting high-quality

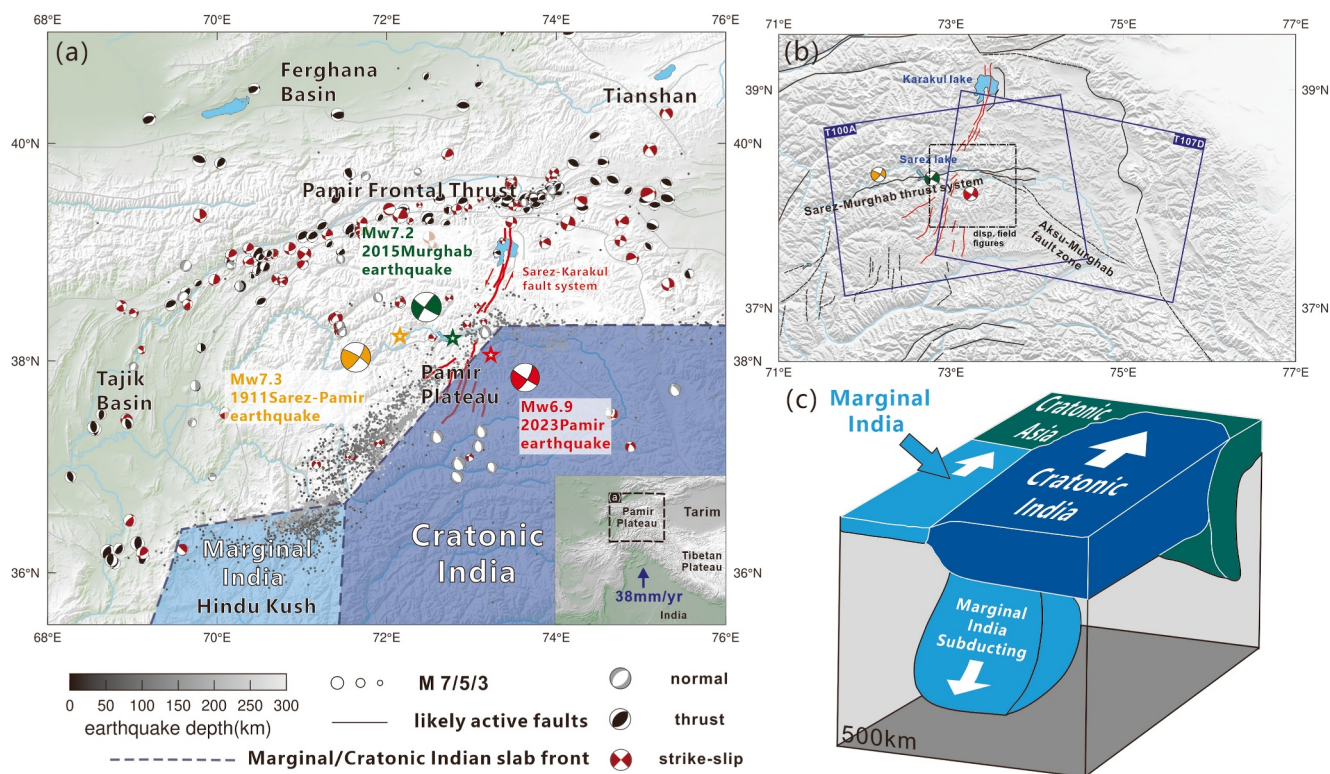


Figure 1. Tectonic background and seismicity distributions. (a) Seismogenic structures and focal mechanisms, with seismic source mechanisms for the 2015 and 2023 earthquakes from USGS, the 1911 earthquake from Kulikova et al. (2016), and additional focal from GCMT and Schurr et al. (2014) and Sippl, Schurr, Yuan, et al. (2013). (b) Detailed view of the study area, showing darkblue boxes that delineate the footprint of Sentinel-1A tracks. The thick green line marks the edge of the underthrusting Indian Plate (Kufner et al., 2018). (c) Plate subduction model for the Pamir Plateau (Kufner et al., 2016).

interferograms spanning the coseismic period (Figure S1 in Supporting Information S1) and their high-coherence regions (Figure S2 in Supporting Information S1), which were then stacked to produce the final deformation field (Figures 2a and 2b, Figure S3 in Supporting Information S1).

To better resolve high-gradient deformation, we additionally used ALOS-2 L-band SAR data. Ascending and descending acquisitions were from 12 and 14 September 2022, and 11 and 13 September 2023, respectively. Processing followed the same workflow as for Sentinel-1, including topographic correction, phase unwrapping, and coherence masking. Multilooking was applied with factors of 2 (azimuth) \times 8 (range). Given the sensitivity of L-band signals to ionospheric effects, we applied ionospheric corrections following Gomba et al. (2016) and Liang et al. (2018).

The final Sentinel-1 LOS displacements reach \sim 20 cm on the descending track and \sim 25 cm on the ascending track, while ALOS-2 data reveal larger displacements of \sim 43 cm (descending) and \sim 41 cm (ascending), highlighting substantial ground deformation associated with the 2023 Tajikistan earthquake (Figures 2c and 2d, Figure S4 in Supporting Information S1). Despite localized decorrelation, the interferograms clearly capture distinct deformation patterns, indicative of predominantly horizontal surface motion. These observations suggest rupture along a northeast-trending strike-slip fault, with left-lateral slip consistent with the earthquake's focal mechanism.

3.2. Slip Model Inversion

We assume that any pre-/post-seismic deformation recorded is negligible, as compared to coseismic displacement such that the resolved slip distribution reveals mostly the coseismic fault rupture. Bayesian inversion was initially employed to constrain the geometric parameters of a single-fault model for this earthquake, the probability density function was constructed using the formula provided by Vasyura-Bathke et al. (2020) (Text S3 in Supporting Information S1). We jointly inverted for slip and fault geometry using the Bayesian Earthquake Analysis Tool (BEAT), which applies an elastic dislocation model (Okada, 1985) and employs Markov Chain Monte Carlo

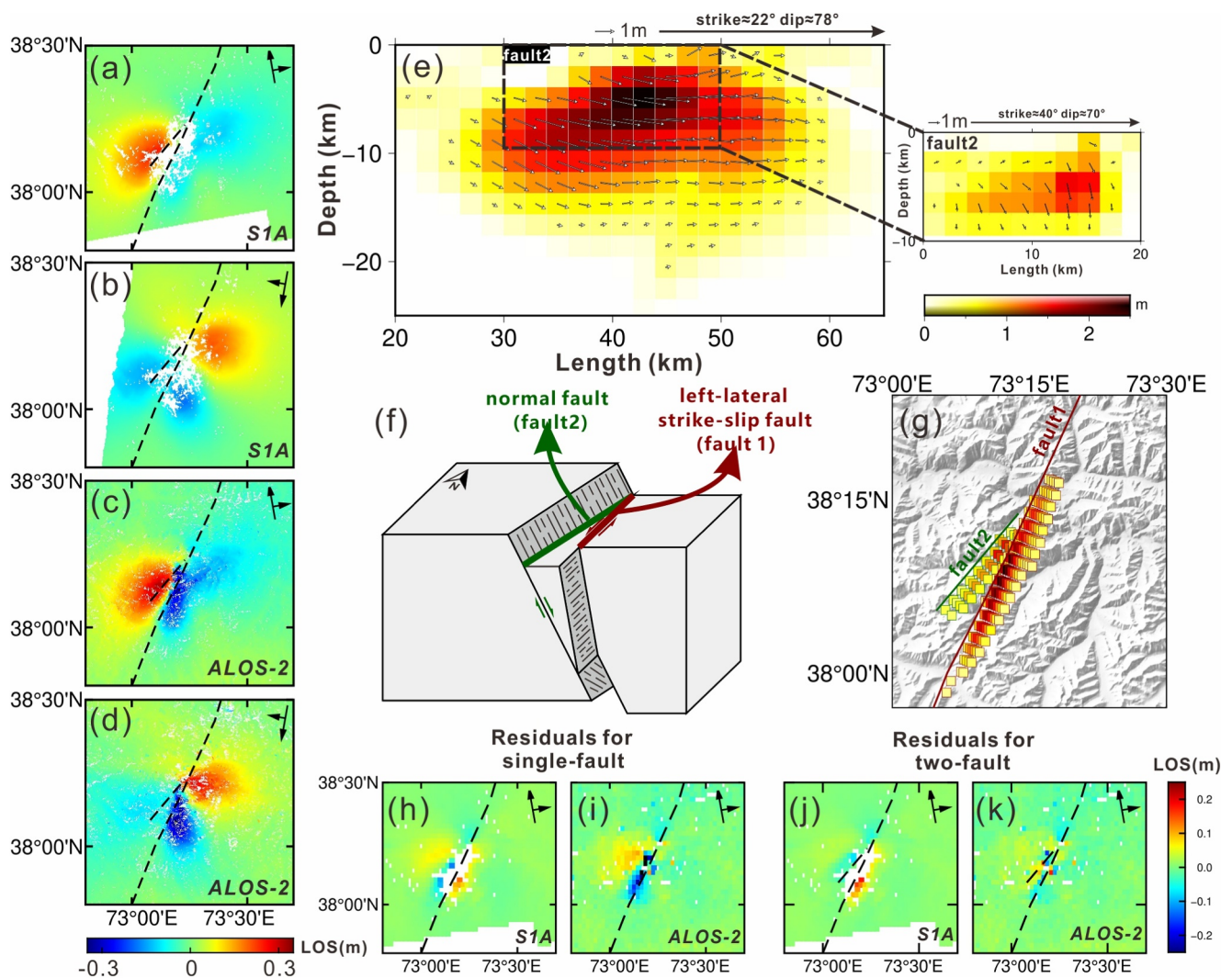


Figure 2. Coseismic InSAR deformation and fault slip model for the 2023 Pamir earthquake. (a–d) Coseismic deformation fields from Sentinel-1A and ALOS-2 ascending and descending tracks. Black dashed lines denote surface fault traces; long and short arrows indicate azimuth and LOS directions, respectively. (e) Plan-view fault slip distribution with slip vectors. (f) Conceptual fault model for the 2023 Pamir earthquake. (g) Surface projection of the modeled slip. (h–k) Residuals of the single-fault and two-fault models from Sentinel-1A and ALOS-2 ascending track data.

sampling to explore source parameters (Heimann et al., 2019; Vasyura-Bathke et al., 2019, 2020, 2021). The fault was simplified as a rectangular plane with uniform slip to facilitate the exploration of geometric parameters (strike, dip, length, and width). Uniform priors within bounds informed by the InSAR pattern and the USGS focal mechanism were applied (see Table S1 in Supporting Information S1 for details).

In the distributed slip inversion, we employed a uniform sampling method to resample the InSAR deformation data, ultimately obtaining 4,226 points from Sentinel-1A ascending track data, 2,400 points from descending track data, 5,442 points from ALOS-2 ascending track data, and 4,291 points from descending track data. Based on the elastic half-space model assumption (Okada, 1985), we inverted the slip distribution using the SDM inversion code constrained by coseismic deformation (R. Wang et al., 2013).

To avoid non-physical oscillations in the slip distribution, a smoothing constraint with a factor of 0.08 was applied during inversion, determined from the slip regularization analysis (Feng et al., 2017, Figure S7 and Text S4 in Supporting Information S1). To determine the optimal fault dip angle, we tested a range of dip angles (70°–90°). The discrepancies between modeled and observed values were further analyzed to assess inversion accuracy.

4. Results

4.1. Slip Model of the 2023 Pamir Mw 6.9 Earthquake

The single-fault Bayesian inversion yields well-constrained, near-normal posterior distributions (Figures S5 and S6 in Supporting Information S1). The probability density reveals a trade-off between depth (4–6 km, referring to the depth to the top of the fault) and slip (Figure S5 in Supporting Information S1), with an uncertainty estimated at approximately ± 1 km. The preferred model features a fault with a dip of 84° , strike of 31° , rake of -8° , length of 23 km, and width of 14 km (Figure S5 in Supporting Information S1), with residuals indicating in Figure S6 in Supporting Information S1.

Building on this model, we performed a single-fault distributed slip inversion. While it improves overall fitting, localized residuals remain—particularly west of the main fault trace—where both ascending Sentinel-1A and ALOS-2 data show deformation anomalies (Figures 2h and 2i), suggesting additional faulting. These anomalies are absent in the descending track, likely due to orbit-specific viewing geometry (Figure S8 in Supporting Information S1). LOS deformation profiles across the main fault residuals (Figure S9 and Text S4 in Supporting Information S1) show consistent step-like signals, confirming the necessity and reliability of a secondary fault. To refine the model, we tested secondary fault geometries across a range of dip angles and identified the optimal configuration by minimizing the RMS misfit between observed and modeled displacements (Figure S10 and Text S4 in Supporting Information S1).

Our preferred two-fault slip model indicates that the 2023 Pamir Mw 6.9 earthquake ruptured two distinct faults (Figure 2e). The main fault exhibits a strike of $\sim 22^\circ$, a dip angle of 78° , and a predominant left-lateral strike-slip motion. The secondary fault is characterized by normal faulting, with a strike of $\sim 40^\circ$ and a dip angle of $\sim 70^\circ$. The slip distribution reveals a maximum slip of 2.5 m on the main fault at a depth of ~ 6 km, while the secondary fault accommodates a maximum slip of 1.5 m at a similar depth. The main fault rupture remarkably reached down to ~ 20 km, which is not common in high plateau (i.e., Tibetan Plateau). This depth extent is required by the observations rather than imposed by smoothing constraints (Text S4 in Supporting Information S1).

This two-fault configuration significantly reduces residuals and effectively reproduces the observed InSAR interferograms without systematic misfit patterns (Figures 2j and 2k). The coseismic deformation is dominated by left-lateral strike-slip motion, consistent with the 2015 Mw 7.2 Murghab earthquake. Overall, the inferred slip distribution is consistent with previously published models (P. He et al., 2024; Shi et al., 2023; S. Wang et al., 2023).

The inversion results reveal the rupture of both a strike-slip fault and a normal fault. Due to the long satellite revisit period, the images captured by ALOS-2 after the earthquake were even obtained about half a year after the earthquake occurred, raising uncertainty as to whether the normal fault rupture occurred coseismically or was triggered by subsequent aftershocks. To evaluate this, we estimated the moment magnitude of the normal fault based on slip model parameters. The resulting magnitude is Mw 6.28 (See Text S5 in Supporting Information S1 for details). Given the absence of any recorded aftershocks with Mw > 6 in either the USGS or GCMT catalogs, we interpret the normal fault rupture as part of the mainshock rather than being aftershock-induced. Huang et al. (2025) explained limited postseismic deformation (maximum 3 cm 4 months after the main shock) by only using afterslip on the main fault, and there is no need for one branch normal fault. Additionally, the comparison between InSAR interferograms with different time baselines also confirmed the limited postseismic deformation (Figure S11 in Supporting Information S1). This minor postseismic deformation aligned with those for the 2015 Murghab earthquake (Jin et al., 2022).

Oblique slip along deep faults can lead to strain partitioning in the upper crust, resulting in simultaneous rupture of faults with different kinematics (Bowman et al., 2003). In this case, deep oblique motion likely generated heterogeneous strain fields, promoting strike-slip and normal faulting through shear and extensional strain accumulation in the shallower crust, respectively. Similar mechanisms have been observed in events such as the 2018 Sulawesi and 2016 Kumamoto earthquakes (Z. He et al., 2020; Kobayashi, 2017; Scott et al., 2019; Song et al., 2019). The 2023 Pamir earthquake reflects a comparable tectonic setting, with co-rupture of strike-slip and normal faults attributed to strain partitioning and stress reorientation. A conceptual model (Figures 2f and 2g) illustrates this process from depth to surface.

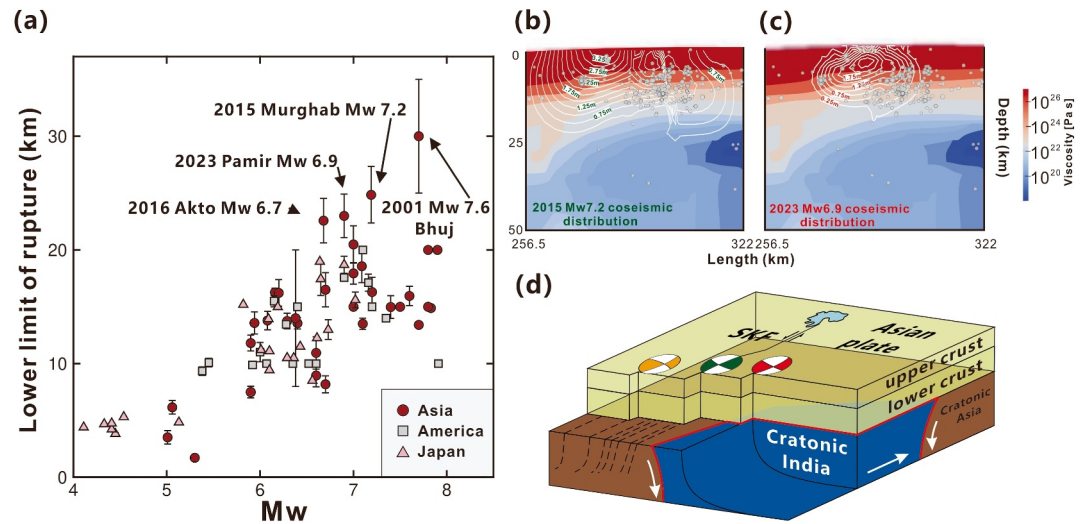


Figure 3. (a) Relationship between earthquake magnitude and rupture depth, the data were collected from previous publications and SRCMOD (See Text S6 and Figure S12 in Supporting Information S1 for details). (b, c) Slip distributions overlain on viscosity profiles for the 2015 Murghab earthquake and the 2023 Tajikistan earthquake, respectively. The viscosity structure across the Pamir region adapted from Sippl, Schurr, Tynpel, et al. (2013). Gray circles represent earthquake hypocenters (Sippl, Schurr, Yuan, et al., 2013). The slip model for the 2015 event is based on Sangha et al. (2017). (d) 3D schematic of the Sarez-Karakul Fault region.

4.2. Comparison to the Previous Slip Models

Geodetic slip models for the 2023 earthquake show significant discrepancies across multiple studies (Table S2 in Supporting Information S1), particularly in the fault location, rupture depth, and slip. Discrepancies among published models stem from both data selection and inversion strategy. Fault geometry is best constrained by two-track InSAR data and resolved by nonlinear inversions, while slip distributions are typically obtained by linear inversion in an elastic half-space, with variations including the use of aftershocks (Chen et al., 2024) and layered velocity models (Huang et al., 2025).

All models agree on left-lateral strike-slip rupture but differ in slip magnitude, depth, and near-surface expression, mainly due to InSAR data quality. Near-field coherence in the Pamir is degraded by high elevation, snow, winter timing, and Sentinel-1's low north-south sensitivity. Masking incoherent pixels can bias models toward surface rupture (P. He et al., 2024), while smoothing choices affect slip magnitude. Z. Liu et al. (2024) inferred rupture to ~15 km, whereas most models, including ours, extend beyond 20 km. Shallow-slip uncertainty is coherence-driven; depth and magnitude differences reflect data quality and inversion regularization.

The existing slip models generally indicate a deep rupture depth. The deeper rupture depth of the 2023 event is similar to that of the 2015 Murghab Mw 7.2 earthquake (Elliott et al., 2020; Jin et al., 2022; Sangha et al., 2017). In the following section, we will explore the implications of these deeper rupture depths in the high Pamir plateau.

5. Discussion

5.1. Enhanced Seismogenic Thickness Due To the Craton Underthrusting

By compiling geodetic slip models of continental earthquakes worldwide (Figure S12 and Text S6 in Supporting Information S1), we found that earthquake rupture depths in the Pamir Plateau, including the 2023 Mw 6.9 Pamir, 2015 Mw 7.2 Murghab, and 2016 Mw 6.7 Akto events, are significantly deeper (Figure 3a). These depths are comparable to those of large earthquakes within the Indian craton, such as the 2001 Mw 7.6 Bhuj earthquake (Copley et al., 2011). We also compared the rupture depth with the local Moho depth (Szwilius et al., 2019) and found no strong correlations. However, earthquakes with rupture depths greater than 20 km generally occur in regions with thicker crust (Jackson et al., 2008, 2021, Figure S12b in Supporting Information S1).

The depth of earthquake rupture is largely governed by crustal rheology, which is controlled by regional geothermal gradients and mineralogical composition (Text S7 in Supporting Information S1). Using 2D

thermomechanical modeling, Sippl, Schurr, Typel, et al. (2013) explored the continental collision dynamics of the Pamir Plateau, revealing a ~25 km thick high-viscosity zone beneath the frontal Pamir (Figure S13 in Supporting Information S1). This high-viscosity structure implies relatively low temperatures and may account for the unusually deep coseismic rupture depths observed near the Sarez-Karakul Fault (SKF). Our observations align with their predictions, providing further evidence for the control of deep lithospheric structure on rupture depth.

To further examine this relationship, we projected the slip distributions of the 2023 Tajikistan and 2015 Murghab earthquakes onto the modeled thermal-viscosity field (Figures 3b and 3c). In both cases, coseismic slip was predominantly concentrated within the high-viscosity zones, suggesting a strong correlation between the thermomechanical structure and the seismogenic behavior.

These findings support the hypothesis that the downward subduction of the Asian cratonic lithosphere, combined with the northward underthrusting of the Indian Plate, reduces temperatures along the plate interface, thereby deepening the brittle–ductile transition. A full 3D geodynamic model would further clarify these interactions and test the proposed mechanism (Figure 3d). Although high strain rates during coseismic rupture process lead to deeper penetration depth, but it cannot account for the large depths observed in the high Pamirs, as large strike-slip events in the Tibetan Plateau—which also involve dynamic strengthening—were confined to ~10 km depth (Yue et al., 2022; D. Zhao et al., 2021).

5.2. The Shear Zone Width in the Interior of Pamir Plateau

The SKF system, acting as a boundary within the Pamir region, separates the sparsely seismic eastern part from the seismically active and intense western part. In addition to the Mw 6.9 2023 earthquake, the SKF system has experienced two other destructive earthquakes during the instrumental, that is, the 1911 Sarez-Pamir M 7.2 and the 2015 Murghab Mw 7.2 events. All these earthquakes were characterized by left-lateral strike-slip movement and ruptured from the near surface down to ~25 km (Table S2 in Supporting Information S1). However, they ruptured different fault segments located tens of kilometers apart, rather than a single strike-slip fault, similar to the SKF segment north of Lake Sarez (Figure 1). This indicates that left-lateral shear strain in the high Pamir Plateau, particularly south of the SMTF system, is distributed across a broad area (S. Wang et al., 2023), spanning at least 150 km based on the distances between the epicenters, rather than being concentrated along a single strike-slip fault plane.

We estimated the shear zone width of the Sarez-Karakul Fault (SKF) by analyzing two ~70 km-wide GNSS velocity profiles across the fault (Figure S14 in Supporting Information S1). Velocity gradients along the P1 profile are observed between ~110 and ~150 km, while the P2 profile shows a broader deformation zone, spanning ~90 to ~200 km—indicative of a longer-wavelength strain distribution (Figure S15 in Supporting Information S1).

To quantify this, we modeled surface deformation using a distribution of infinitesimal screw dislocations (Text S8 in Supporting Information S1, Miller et al., 2024; Prescott & Nur, 1981), which allows estimation of shear zone width. Results show that the shear zone at the P1 transect is ~33 km wide, while at P2 it reaches ~193 km, suggesting distributed strain accommodated by multiple parallel fault strands in the southern segment (Figure 4). This interpretation is supported by a complementary elastic half-space dislocation model assuming an infinitely long and deep fault (Text S9 in Supporting Information S1, Savage & Burford, 1973), which yields consistent results (Figure S16 in Supporting Information S1).

In addition, the broad distribution of seismicity along the P2 profile suggests more distributed deformation south of the SMTF, in contrast to the more localized faulting observed to the north (Figure 4). However, the sparse GNSS coverage and uncertainties in earthquake locations limit the ability to resolve internal deformation structures; thus, a set of localized shear zones or subsidiary faults may contribute to the broad shear zone south of the SMTF.

We propose that the underthrusting craton plays a key role in the formation and persistence of the broad shear zone in the High Pamir Plateau. The thickened lithosphere beneath the High Pamirs likely retains more heat due to tectonic thickening (Sippl, Schurr, Typel, et al., 2013), reducing lithospheric strength and favoring distributed deformation. In contrast, the cold and rigid Asian cratonic lithosphere advancing beneath the northern Pamirs

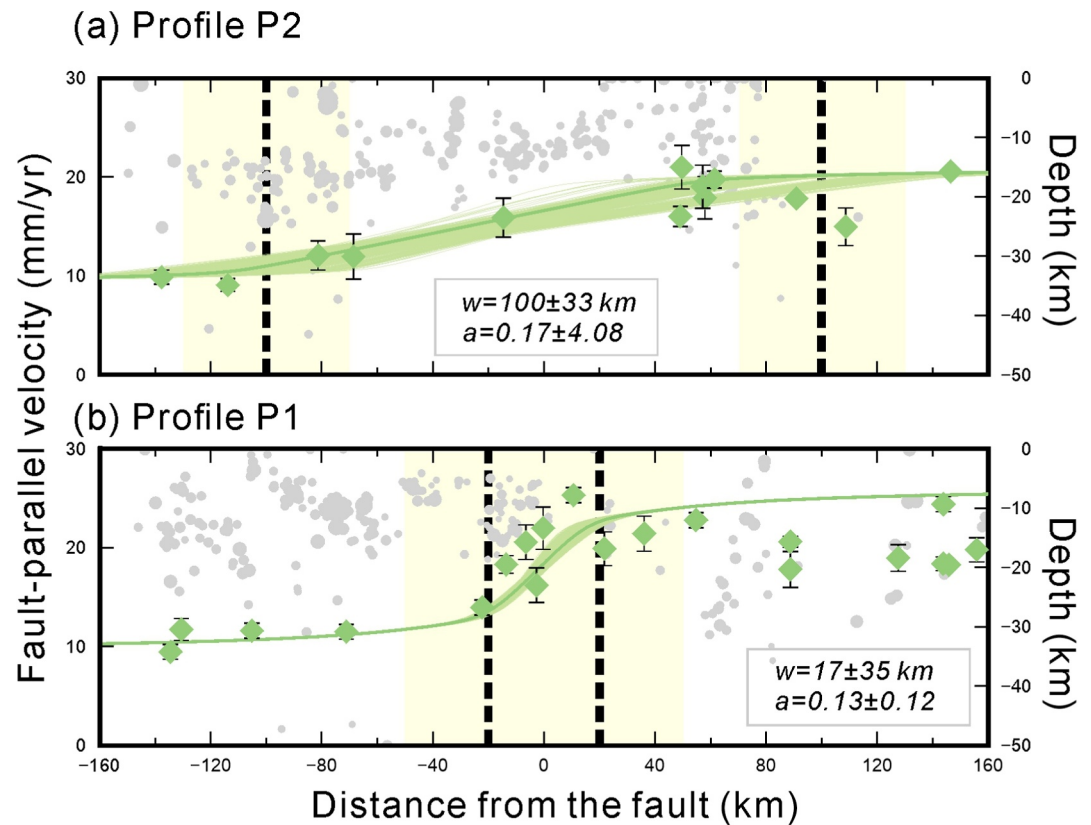


Figure 4. Shear zone width of the Sarez-Karakul Fault System constrained by GNSS data along (a) the P2 profile and (b) the P1 profile. The variable “a” represents the horizontal shift factor, while “w” denotes the half-width of the shear zone. Gray dots indicate relocated earthquakes from Sippl, Schurr, Yuan, et al. (2013). Dashed lines delineate the boundaries of the shear zone and the transparent yellow box illustrates the corresponding uncertainties in the shear zone width.

cools and strengthens the overlying crust, promoting fault localization in that region. This framework is consistent with the observed diffuse seismicity and broad interseismic strain patterns across the interior Pamir Plateau.

6. Conclusions

The 2023 Mw 6.9 Pamir earthquake involved strain partitioned fault system—a left-lateral strike-slip and a normal fault. The deep rupture (~20 km), consistent with the 2015 Murghab earthquake, reflects the strengthening effect of the cold, underthrusting Asian craton, which cools and stiffens the upper crust, pushing seismicity deeper than those in the nearby Tibetan Plateau. The broad distribution of shear strain across the High Pamir, evidenced by consistent strike-slip mechanisms in historical earthquakes, is controlled by the mechanical interaction between the underthrusting cratonic plate and the Pamir lithosphere. This deep lithospheric structure governs both rupture depth and deformation style, highlighting its key role in shaping the region's seismic behavior and tectonic evolution.

Conflict of Interest

The authors declare no conflicts of interest relevant to this study.

Data Availability Statement

The data used in this study are available on Zenodo (Q. Liu et al., 2025). The BEAT code can be accessed from GitHub at <https://pyrocko.org/beat/docs/current/index.html>. Finite slip models for continental earthquakes globally were collected from <http://equake-rc.info/srcmod/>. Maps were generated using Generic Mapping Tools (GMT) version 6 (Wessel et al., 2019).

Acknowledgments

We acknowledge the constructive comments provided by Editor Daoyuan Sun and reviewers Romain Jolivet, Iskander Muldashev, and anonymous reviewer during the revision of our manuscript. Yingfeng Zhang was funded by the National Key Research and Development Program of China (Grant 2022YFC3003700) and by the Basic Scientific Funding of the Institute of Geology, China Earthquake Administration (IGCEA1809). Luca Dal Zilio was supported by the Earth Observatory of Singapore (EOS), and the Singapore Ministry of Education Tier 3b project "Investigating Volcano and Earthquake Science and Technology (InVEST)" (Award MOE-MOET32021-0002).

References

- Bai, L., & Zhang, T. (2015). Complex deformation pattern of the Pamir–Hindu Kush region inferred from multi-scale double-difference earthquake relocations. *Tectonophysics*, *638*, 177–184. <https://doi.org/10.1016/j.tecto.2014.11.006>
- Bloch, W., Metzger, S., Schurr, B., Yuan, X., Ratschbacher, L., Reuter, S., et al. (2023). The 2015–2017 Pamir earthquake sequence: Foreshocks, main shocks and aftershocks, seismotectonics, fault interaction and fluid processes. *Geophysical Journal International*, *233*(1), 641–662. <https://doi.org/10.1093/gji/ggac473>
- Bloch, W., Schurr, B., Yuan, X., Ratschbacher, L., Reuter, S., Kufner, S. K., et al. (2021). Structure and stress field of the lithosphere between Pamir and Tarim. *Geophysical Research Letters*, *48*(22), e2021GL095413. <https://doi.org/10.1029/2021GL095413>
- Bowman, D., King, G., & Tapponnier, P. (2003). Slip partitioning by elastoplastic propagation of oblique slip at depth. *Science*, *300*(5622), 1121–1123. <https://doi.org/10.1126/science.1082180>
- Burtman, V. S., & Molnar, P. (1993). Geological and geophysical evidence for deep subduction of continental crust beneath the Pamir. <https://doi.org/10.1130/SPE281-p1>
- Chen, R., Li, J., Liu, D., Yushan, A., Li, R., & Kong, X. (2024). InSAR coseismic deformation and seismogenic structure of the 2023 Mw6.9 Tajikistan earthquake. *Geodesy and Geodynamics*, *16*(5), 579–590. <https://doi.org/10.1016/j.geog.2023.12.004>
- Copley, A., Avouac, J. P., Hollingsworth, J., & Leprince, S. (2011). The 2001 Mw 7.6 Bhuj earthquake, low fault friction, and the crustal support of plate driving forces in India. *Journal of Geophysical Research*, *116*(B8), B08405. <https://doi.org/10.1029/2010JB008137>
- Cowgill, E. (2010). Cenozoic right-slip faulting along the eastern margin of the Pamir salient, northwestern China. *Bulletin*, *122*(1–2), 145–161. <https://doi.org/10.1130/B26520.1>
- Dal Zilio, L., van Dinther, Y., Gerya, T., & Avouac, J. P. (2019). Bimodal seismicity in the Himalaya controlled by fault friction and geometry. *Nature Communications*, *10*(1), 48. <https://doi.org/10.1038/s41467-018-07874-8>
- Elliott, A., Elliott, J., Hollingsworth, J., Kulikova, G., Parsons, B., & Walker, R. (2020). Satellite imaging of the 2015 M 7.2 earthquake in the Central Pamir, Tajikistan, elucidates a sequence of shallow strike-slip ruptures of the Sarez-Karakul fault. *Geophysical Journal International*, *221*(3), 1696–1718. <https://doi.org/10.1093/gji/ggaa090>
- Fan, G., Ni, J. F., & Wallace, T. C. (1994). Active tectonics of the Pamirs and Karakorum. *Journal of Geophysical Research*, *99*(B4), 7131–7160. <https://doi.org/10.1029/93JB02970>
- Feng, W., Samsonov, S., Tian, Y., Qiu, Q., Li, P., Zhang, Y., et al. (2017). Surface deformation associated with the 2015 Mw 8.3 Illapel earthquake revealed by satellite-based geodetic observations and its implications for the seismic cycle. *Earth and Planetary Science Letters*, *460*, 222–233. <https://doi.org/10.1016/j.epsl.2016.11.018>
- Gomba, G., González, F. R., & De Zan, F. (2016). Ionospheric phase screen compensation for the Sentinel-1 TOPS and ALOS-2 ScanSAR modes. *IEEE Transactions on Geoscience and Remote Sensing*, *55*(1), 223–235. <https://doi.org/10.1109/TGRS.2016.2604461>
- He, P., Wen, Y., Wang, X., & Cai, J. (2024). The NS direction strike-slip activities in the Pamir hinterland under oblique convergence: The 2015 and 2023 earthquakes. *Geophysical Journal International*, *238*(2), 1150–1163. <https://doi.org/10.1093/gji/ggae214>
- He, Z., Chen, T., Wang, M., & Li, Y. (2020). Multi-segment rupture model of the 2016 Kumamoto earthquake revealed by InSAR and GPS data. *Remote Sensing*, *12*(22), 3721. <https://doi.org/10.3390/rs12223721>
- Heimann, S., Vasyura-Bathke, H., Sudhaus, H., Isken, M. P., Kriegerowski, M., Steinberg, A., & Dahm, T. (2019). A Python framework for efficient use of pre-computed Green's functions in seismological and other physical forward and inverse source problems. *Solid Earth*, *10*(6), 1921–1935. <https://doi.org/10.5194/se-10-1921-2019>
- Huang, X., Jolivet, R., Li, Y., Shan, X., & Raimbault, B. (2025). The 2023 Mw 6.9 Sarez, Tajikistan earthquake: Subparallel faulting and distributed deformation of the Pamir. *Geophysical Journal International*, *240*(3), 1790–1801. <https://doi.org/10.1093/gji/ggae404>
- Jackson, J., McKenzie, D., & Priestley, K. (2021). Relations between earthquake distributions, geological history, tectonics and rheology on the continents. *Philosophical Transactions of the Royal Society A*, *379*(2193), 20190412. <https://doi.org/10.1098/rsta.2019.0412>
- Jackson, J., McKenzie, D. A. N., Priestley, K., & Emmerson, B. (2008). New views on the structure and rheology of the lithosphere. *Journal of the Geological Society*, *165*(2), 453–465. <https://doi.org/10.1144/0016-76492007-109>
- Jin, Z., Fialko, Y., Zubovich, A., & Schöne, T. (2022). Lithospheric deformation due to the 2015 M7.2 Sarez (Pamir) earthquake constrained by 5 years of space geodetic observations. *Journal of Geophysical Research: Solid Earth*, *127*(4), e2021JB022461. <https://doi.org/10.1029/2021JB022461>
- Kobayashi, T. (2017). Earthquake rupture properties of the 2016 Kumamoto earthquake foreshocks (Mj 6.5 and Mj 6.4) revealed by conventional and multiple-aperture InSAR. *Earth Planets and Space*, *69*(1), 7. <https://doi.org/10.1186/s40623-016-0594-y>
- Kufner, S. K., Schurr, B., Ratschbacher, L., Murodkulov, S., Abdulhameed, S., Ischuk, A., et al. (2018). Seismotectonics of the Tajik basin and surrounding mountain ranges. *Tectonics*, *37*(8), 2404–2424. <https://doi.org/10.1029/2017TC004812>
- Kufner, S. K., Schurr, B., Sippl, C., Yuan, X., Ratschbacher, L., Ischuk, A., et al. (2016). Deep India meets deep Asia: Lithospheric indentation, delamination and break-off under Pamir and Hindu Kush (central Asia). *Earth and Planetary Science Letters*, *435*, 171–184. <https://doi.org/10.1016/j.epsl.2015.11.046>
- Kulikova, G., Schurr, B., Krüger, F., Brzoska, E., & Heimann, S. (2016). Source parameters of the Sarez-Pamir earthquake of 1911 February 18. *Geophysical Journal International*, *205*(2), 1086–1098. <https://doi.org/10.1093/gji/ggw069>
- Lavier, L. L., Tong, X., & Biemiller, J. (2021). The mechanics of creep, slow slip events, and earthquakes in mixed brittle-ductile fault zones. *Journal of Geophysical Research: Solid Earth*, *126*(2), e2020JB020325. <https://doi.org/10.1029/2020JB020325>
- Liang, C., Liu, Z., Fielding, E. J., & Bürgmann, R. (2018). InSAR time series analysis of L-band wide-swath SAR data acquired by ALOS-2. *IEEE Transactions on Geoscience and Remote Sensing*, *56*(8), 4492–4506. <https://doi.org/10.1109/TGRS.2018.2821150>
- Liu, Q., Zhang, Y., Ma, Z., Dal Zilio, L., Zhang, G., Li, H., & Shan, X. (2025). Seismogenic thickening in the Pamir Plateau from craton underthrusting revealed by the 2023 Mw 6.9 earthquake: Supporting_information [Dataset]. *Zenodo*. <https://doi.org/10.5281/zenodo.17211913>
- Liu, Z., Li, Z., Yu, C., Zhang, X., & Peng, J. (2024). Stress triggering and future seismic hazards implied by four large earthquakes in the Pamir from 2015 to 2023 revealed by Sentinel-1 radar interferometry. *Geophysical Journal International*, *237*(2), 887–901. <https://doi.org/10.1093/gji/ggae079>
- Ma, Z. F., Jiang, M., & Huang, T. (2020). A sequential approach for Sentinel-1 TOPS time-series co-registration over low coherence scenarios. *IEEE Transactions on Geoscience and Remote Sensing*, *59*(6), 4818–4826. <https://doi.org/10.1109/TGRS.2020.3009996>
- Ma, Z. F., Jiang, M., Khoshmanesh, M., & Cheng, X. (2021). Time series phase unwrapping based on graph theory and compressed sensing. *IEEE Transactions on Geoscience and Remote Sensing*, *60*, 1–12. <https://doi.org/10.1109/TGRS.2021.3066784>
- Ma, Z. F., Jiang, M., Zhao, Y., Malhotra, R., & Yong, B. (2019). Minimum spanning tree co-registration approach for time-series Sentinel-1 TOPS data. *IEEE Journal of Selected Topics in Applied Earth Observations and Remote Sensing*, *12*(8), 3004–3013. <https://doi.org/10.1109/JSTARS.2019.2920717>

- Ma, Z. F., Liu, J., Aoki, Y., Wei, S., Liu, X., Cui, Y., et al. (2022). Towards big SAR data era: An efficient Sentinel-1 near-real-time InSAR processing workflow with an emphasis on co-registration and phase unwrapping. *ISPRS Journal of Photogrammetry and Remote Sensing*, *188*, 286–300. <https://doi.org/10.1016/j.isprsjprs.2022.04.013>
- Miller, N. M., Kreemer, C., Hammond, W. C., & Blewitt, G. (2024). Geodetic evidence for distributed shear below the brittle crust of the Walker Lane, western United States. *Journal of Geophysical Research: Solid Earth*, *129*(9), e2024JB028848. <https://doi.org/10.1029/2024JB028848>
- Murphy, M. A., Yin, A., Kapp, P., Harrison, T. M., Lin, D., & Jinghui, G. (2000). Southward propagation of the Karakoram fault system, southwest Tibet: Timing and magnitude of slip. *Geology*, *28*(5), 451–454. [https://doi.org/10.1130/0091-7613\(2000\)28<451:spotkf>2.0.co;2](https://doi.org/10.1130/0091-7613(2000)28<451:spotkf>2.0.co;2)
- Okada, Y. (1985). Surface deformation due to shear and tensile faults in a half-space. *Bulletin of the Seismological Society of America*, *75*(4), 1135–1154. <https://doi.org/10.1785/BSSA0750041135>
- Pegler, G., & Das, S. (1998). An enhanced image of the Pamir–Hindu Kush seismic zone from relocated earthquake hypocenters. *Geophysical Journal International*, *134*(2), 573–595. <https://doi.org/10.1046/j.1365-246x.1998.00582.x>
- Perry, M., Kakar, N., Ischuk, A., Metzger, S., Bendick, R., Molnar, P., & Mohadjer, S. (2019). Little geodetic evidence for localized Indian subduction in the Pamir-Hindu Kush of central Asia. *Geophysical Research Letters*, *46*(1), 109–118. <https://doi.org/10.1029/2018GL080065>
- Prescott, W. H., & Nur, A. (1981). The accommodation of relative motion at depth on the San Andreas fault system in California. *Journal of Geophysical Research*, *86*(B2), 999–1004. <https://doi.org/10.1029/JB086iB02p00999>
- Rutte, D., Ratschbacher, L., Schneider, S., Stübner, K., Stearns, M. A., Gulzar, M. A., & Hacker, B. R. (2017). Building the Pamir-Tibetan Plateau—Crustal stacking, extensional collapse, and lateral extrusion in the central Pamir: 1. Geometry and kinematics. *Tectonics*, *36*(3), 342–384. <https://doi.org/10.1002/2016TC004293>
- Sangha, S., Peltzer, G., Zhang, A., Meng, L., Liang, C., Lundgren, P., & Fielding, E. (2017). Fault geometry of 2015, Mw7.2 Murghab, Tajikistan earthquake controls rupture propagation: Insights from InSAR and seismological data. *Earth and Planetary Science Letters*, *462*, 132–141. <https://doi.org/10.1016/j.epsl.2017.01.018>
- Savage, J. C., & Burford, R. O. (1973). Geodetic determination of relative plate motion in central California. *Journal of Geophysical Research*, *78*(5), 832–845. <https://doi.org/10.1029/JB078i005p00832>
- Schurr, B., Ratschbacher, L., Sippl, C., Gloguen, R., Yuan, X., & Mechie, J. (2014). Seismotectonics of the Pamir. *Tectonics*, *33*(8), 1501–1518. <https://doi.org/10.1002/2014TC003576>
- Schwab, M., Ratschbacher, L., Siebel, W., McWilliams, M., Minaev, V., Lutkov, V., et al. (2004). Assembly of the Pamirs: Age and origin of magmatic belts from the southern Tien Shan to the southern Pamirs and their relation to Tibet. *Tectonics*, *23*(4), TC4002. <https://doi.org/10.1029/2003TC001583>
- Scott, C., Champenois, J., Klinger, Y., Nissen, E., Maruyama, T., Chiba, T., & Arrowsmith, R. (2019). The 2016 M7 Kumamoto, Japan, earthquake slip field derived from a joint inversion of differential LiDAR topography, optical correlation, and InSAR surface displacements. *Geophysical Research Letters*, *46*(12), 6341–6351. <https://doi.org/10.1029/2019GL082202>
- Shi, Y., Wang, Y., & Bian, Y. (2023). Coseismic source model of the February 2023 Mw 6.8 Tajikistan earthquake from Sentinel-1A InSAR observations and its associated earthquake hazard. *Remote Sensing*, *15*(12), 3010. <https://doi.org/10.3390/rs15123010>
- Sippl, C., Schurr, B., Tjypel, J., Angiboust, S., Mechie, J., Yuan, X., et al. (2013). Deep burial of Asian continental crust beneath the Pamir imaged with local earthquake tomography. *Earth and Planetary Science Letters*, *384*, 165–177. <https://doi.org/10.1016/j.epsl.2013.10.013>
- Sippl, C., Schurr, B., Yuan, X., Mechie, J., Schneider, F. M., Gadoev, M., et al. (2013). Geometry of the Pamir-Hindu Kush intermediate-depth earthquake zone from local seismic data. *Journal of Geophysical Research: Solid Earth*, *118*(4), 1438–1457. <https://doi.org/10.1002/jgrb.50128>
- Song, X., Zhang, Y., Shan, X., Liu, Y., Gong, W., & Qu, C. (2019). Geodetic observations of the 2018 Mw 7.5 Sulawesi earthquake and its implications for the kinematics of the Palu fault. *Geophysical Research Letters*, *46*(8), 4212–4220. <https://doi.org/10.1029/2019GL082045>
- Strecker, M. R., Frisch, W., Hamburger, M. W., Ratschbacher, L., Semiletkin, S., Zamoruyev, A., & Sturchio, N. (1995). Quaternary deformation in the eastern Pamirs, Tadjikistan and Kyrgyzstan. *Tectonics*, *14*(5), 1061–1079. <https://doi.org/10.1029/95TC00927>
- Szwilius, W., Afonso, J. C., Ebbing, J., & Mooney, W. D. (2019). Global crustal thickness and velocity structure from geostatistical analysis of seismic data. *Journal of Geophysical Research: Solid Earth*, *124*(2), 1626–1652. <https://doi.org/10.1029/2018JB016593>
- Vasyura-Bathke, H., Dettmer, J., Dutta, R., Mai, P. M., & Jonsson, S. (2021). Accounting for theory errors with empirical Bayesian noise models in nonlinear centroid moment tensor estimation. *Geophysical Journal International*, *225*(2), 1412–1431. <https://doi.org/10.1093/gji/ggab034>
- Vasyura-Bathke, H., Dettmer, J., Steinberg, A., Heimann, S., Isken, M. P., Zielke, O., et al. (2019). BEAT: Bayesian earthquake analysis tool. <https://doi.org/10.5880/fidgeo.2019.024>
- Vasyura-Bathke, H., Dettmer, J., Steinberg, A., Heimann, S., Isken, M. P., Zielke, O., et al. (2020). The Bayesian earthquake analysis tool. *Seismological Research Letters*, *91*(2A), 1003–1018. <https://doi.org/10.1785/02201900075>
- Wang, R., Diao, F., & Hoechner, A. (2013). SDM-A geodetic inversion code incorporating with layered crust structure and curved fault geometry. In *EGU general assembly conference abstracts. (EGU2013-2411)*.
- Wang, S., Song, C., & Xiao, Z. (2023). Two $m_w \geq 6.5$ earthquakes in central Pamir constrained by satellite SAR observations. *Remote Sensing*, *15*(21), 5115. <https://doi.org/10.3390/rs15215115>
- Wang, S., Tang, W., Liu, Y., Liu, X., & Yao, X. (2020). Rushan-Pshart Paleo-Tethyan suture deduced from geochronological, geochemical, and Sr-Nd-Hf isotopic characteristics of granitoids in Pamir. *Lithos*, *364–365*, 105549. <https://doi.org/10.1016/j.lithos.2020.105549>
- Wessel, P., Luis, J. F., Uieda, L., Scharroo, R., Wobbe, F., Smith, W. H. F., & Tian, D. (2019). The generic mapping tools version 6. *Geochemistry, Geophysics, Geosystems*, *20*(11), 5556–5564. <https://doi.org/10.1029/2019GC008515>
- Yin, A., Robinson, A., & Manning, C. E. (2001). Oroclinal bending and slab-break-off causing coeval east-west extension and east-west contraction in the Pamir-Nanga Parbat syntaxis in the past 10 my. In *AGU fall meeting abstracts* (Vol. 2001, p. T12F-03).
- Yue, H., Shen, Z.-K., Zhao, Z., Wang, T., Cao, B., Li, Z., et al. (2022). Rupture process of the 2021 M7.4 Maduo earthquake and implication for deformation mode of the Songpan-Ganzi terrane in Tibetan Plateau. *Proceedings of the National Academy of Sciences of the United States of America*, *119*(23), e2116445119. <https://doi.org/10.1073/pnas.2116445119>
- Zhan, Z., & Kanamori, H. (2016). Recurring large deep earthquakes in Hindu Kush driven by a sinking slab. *Geophysical Research Letters*, *43*(14), 7433–7441. <https://doi.org/10.1002/2016GL069603>
- Zhang, J., Shan, X., & Huang, X. (2011). Seismotectonics in the Pamir: An oblique transpressional shear and south-directed deep-subduction model. *Geoscience Frontiers*, *2*(1), 1–15. <https://doi.org/10.1016/j.gsf.2010.11.002>
- Zhao, D., Qu, C., Bürgmann, R., Gong, W., & Shan, X. (2021). Relaxation of Tibetan lower crust and afterslip driven by the 2001 Mw7.8 Kokoxili. *China, Earthquake Constrained by a Decade of Geodetic Measurements*, *126*(4), e2020JB021314. <https://doi.org/10.1029/2020JB021314>

Zhao, J., Zhang, P., Zhang, X., Yuan, X., Kind, R., van der Hilst, R., et al. (2021). Crust-mantle structure and geodynamic processes in western China and their constraints on resources and environment: Research progress of the ANTILOPE project. *Earth Science Frontiers*, 28(5), 230–259. <https://doi.org/10.13745/j.esf.sf.2021.9.38>

References From the Supporting Information

- Blanpied, M. L., Lockner, D. A., & Byerlee, J. D. (1995). Frictional slip of granite at hydrothermal conditions. *Journal of Geophysical Research*, 100(B7), 13045–13064. <https://doi.org/10.1029/95JB00862>
- Chen, W.-P., & Molnar, P. (1983). Focal depths of intracontinental and intraplate earthquakes and their implications for the thermal and mechanical properties of the lithosphere. *Journal of Geophysical Research*, 88(B5), 4183–4214. <https://doi.org/10.1029/JB088iB05p04183>
- Di, N., Li, C., Li, T., Hu, W., Chen, Z., Zhang, Y., et al. (2023). The 2021 Mw 5.2 Baicheng earthquake: Implications for the hazards of extremely shallow earthquakes. *Seismological Research Letters*, 94(4), 1775–1790. <https://doi.org/10.1785/0220220328>
- Dong, Y., Meng, G., & Hong, S. (2020). Coseismic and postseismic deformation of the 2016 Mw 6.6 Aketao earthquake from InSAR observations and modelling. *Pure and Applied Geophysics*, 177(1), 265–283. <https://doi.org/10.1007/s00024-019-02092-9>
- Han, B., Liu, Z., Chen, B., Li, Z., Yu, C., Zhang, Y., & Peng, J. (2022). Coseismic deformation and slip distribution of the 2022 Luding Mw 6.6 earthquake revealed by InSAR observations. *Wuhan Daxue Xuebao (Xinxi Kexue Ban)/Geomatics and Information Science of Wuhan University*, 1, 1–13. <https://doi.org/10.13203/j.whugis20220636>
- Hong-Wei, T., Rong-Jiang, W., Fa-Qi, D., Yong, Z., Yong-Ge, W., & Ming-Pei, J. (2016). Slip model of the 2001 Kunlun Mountain MS8.1 earthquake by SDM: Joint inversion from GPS and InSAR data. *Chinese Journal of Geophysics*, 59(4), 404–413. <https://doi.org/10.1002/cjg2.20245>
- Ischuk, A., Bendick, R., Rybin, A., Molnar, P., Khan, S. F., Kuzikov, S., et al. (2013). Kinematics of the Pamir and Hindu Kush regions from GPS geodesy. *Journal of Geophysical Research: Solid Earth*, 118(5), 2408–2416. <https://doi.org/10.1002/jgrb.50185>
- Jónsson, S. N., Zebker, H., Segall, P., & Amelung, F. (2002). Fault slip distribution of the 1999 Mw 7.1 Hector mine, California, earthquake, estimated from satellite radar and GPS measurements. *Bulletin of the Seismological Society of America*, 92(4), 1377–1389. <https://doi.org/10.1785/0120000922>
- Jouanne, F., Awan, A., Pêcher, A., Kausar, A., Mugnier, J. L., Khan, I., et al. (2014). Present-day deformation of northern Pakistan from salt ranges to Karakorum ranges. *Journal of Geophysical Research: Solid Earth*, 119(3), 2487–2503. <https://doi.org/10.1002/2013JB010776>
- Kanamori, H. (1977). The energy release in great earthquakes. *Journal of Geophysical Research*, 82(20), 2981–2987. <https://doi.org/10.1029/JB082i020p02981>
- Luo, H., Wang, T., & Wei, S. (2022). Systematic comparison of InSAR and seismic source models for moderate-size earthquakes in Western China: Implication to the seismogenic capacity of the shallow crust. *Journal of Geophysical Research: Solid Earth*, 127(10), e2022JB024794. <https://doi.org/10.1029/2022JB024794>
- Lythgoe, K., Muzli, M., Bradley, K., Wang, T., Nugraha, A. D., Zulfakriza, Z., et al. (2021). Thermal squeezing of the seismogenic zone controlled rupture of the volcano-rooted Flores Thrust. *Science Advances*, 7(5), eabe2348. <https://doi.org/10.1126/sciadv.abe2348>
- Metzger, S., Gagala, E., Ratschbacher, L., Lazecký, M., Maghsoudi, Y., & Schurr, B. (2021). Tajik depression and greater Pamir neotectonics from InSAR rate maps. *Journal of Geophysical Research: Solid Earth*, 126(12), e2021JB022775. <https://doi.org/10.1029/2021JB022775>
- Muldashev, I. A., Pérez-Gussinyé, M., & Sobolev, S. V. (2022). Modeling of Continental normal fault earthquakes. *Geochemistry, Geophysics, Geosystems*, 23(12), e2022GC010615. <https://doi.org/10.1029/2022GC010615>
- Qiao, X., Wang, Q., Yang, S., Li, J., Zou, R., & Ding, K. (2015). The 2008 Nura Mw6.7 earthquake: A shallow rupture on the main Pamir thrust revealed by GPS and InSAR. *Geodesy and Geodynamics*, 6(2), 91–100. <https://doi.org/10.1016/j.geog.2015.01.005>
- Scholz, C. H. (1988). The brittle-plastic transition and the depth of seismic faulting. *Geologische Rundschau*, 77(1), 319–328. <https://doi.org/10.1007/BF01848693>
- Thingbaijam, K. K. S., Martin Mai, P., & Goda, K. (2017). New empirical earthquake source-scaling laws. *Bulletin of the Seismological Society of America*, 107(5), 2225–2246. <https://doi.org/10.1785/0120170017>
- Vernant, P. (2015). What can we learn from 20 years of interseismic GPS measurements across strike-slip faults? *Tectonophysics*, 644, 22–39. <https://doi.org/10.1016/j.tecto.2015.01.013>
- Wells, D. L., & Coppersmith, K. J. (1994). New empirical relationships among magnitude, rupture length, rupture width, rupture area, and surface displacement. *Bulletin of the Seismological Society of America*, 84(4), 974–1002. <https://doi.org/10.1785/BSSA0840040974>
- Werner, C., Wegmüller, U., Strozzi, T., & Wiesmann, A. (2002). Processing strategies for phase unwrapping for INSAR applications. In *Proceedings of the European conference on synthetic aperture radar (EUSAR 2002)* (Vol. 1, pp. 353–356).
- Xia, B., Artemieva, I. M., Thybo, H., & Klempner, S. L. (2023). Strong variability in the thermal structure of Tibetan lithosphere. *Journal of Geophysical Research: Solid Earth*, 128(3), e2022JB026213. <https://doi.org/10.1029/2022JB026213>
- Xin-Jian, S., Chun-Yan, Q. U., Wen-Yu, G., De-Zheng, Z., Ying-Feng, Z., Guo-Hong, Z., et al. (2017). Coseismic deformation field of the Jiuzhaigou MS7.0 earthquake from Sentinel-1A InSAR data and fault slip inversion. *Chinese Journal of Geophysics*, 60(12), 4527–4536. <https://doi.org/10.6038/cjg20171201>
- Yanfang, D., Guojie, M., & Shunying, H. (2022). Coseismic deformation and slip distribution of the 2017 Mw 6.3 Jinghe, Xinjiang, western China earthquake based on InSAR observations: A buried reverse event on previously unknown fault. *Geophysical Journal International*, 230(3), 2147–2161. <https://doi.org/10.1093/gji/ggac170>
- Yang, J., Xu, C., & Wen, Y. (2023). Coseismic and early postseismic deformation associated with the January 2022 Mw 6.6 Menyuan earthquake, NE Tibet, revealed by InSAR observations. *Tectonophysics*, 868, 230090. <https://doi.org/10.1016/j.tecto.2023.230090>
- Yun-Hua, L. I. U., Chi-Sheng, W., Xin-Jian, S., Gui-Fang, Z., & Chun-Yan, Q. U. (2014). Result of SAR differential interferometry for the coseismic deformation and source parameter of the MS7.0 Lushan earthquake. *Chinese Journal of Geophysics*, 57(8), 2495–2506. <https://doi.org/10.6038/cjg20140811>
- Zhang, Z., Wu, S., Zhang, B., Du, Z., & Xia, Q. (2024). The distribution of surface heat flow on the Tibetan Plateau revealed by data-driven. *Methods*, 129(10), e2023JB028491. <https://doi.org/10.1029/2023JB028491>
- Zheng, G., Wang, H., Wright, T. J., Lou, Y., Zhang, R., Zhang, W., et al. (2017). Crustal deformation in the India-Eurasia collision zone from 25 years of GPS measurements. *Journal of Geophysical Research: Solid Earth*, 122(11), 9290–9312. <https://doi.org/10.1002/2017JB014465>
- Zhou, Y., He, J., Oimahmadov, I., Gadoev, M., Pan, Z., Wang, W., et al. (2016). Present-day crustal motion around the Pamir Plateau from GPS measurements. *Gondwana Research*, 35, 144–154. <https://doi.org/10.1016/j.gr.2016.03.011>
- Zubovich, A. V., Wang, X.-Q., Scherba, Y. G., Schelochkov, G. G., Reilinger, R., Reigber, C., et al. (2010). GPS velocity field for the Tien Shan and surrounding regions. *Tectonics*, 29(6), TC6014. <https://doi.org/10.1029/2010TC002772>